Turbulent Flow in an Isosceles Triangular Duct

By Hiromoto USUI*, Yuji SANO* and Shigeru OKADA**

(Received July 15, 1983)

Abstract

Fully developed turbulent flow characteristics in an isosceles triangular duct with a narrow apex angle were measured by means of a hot wire anemometer. Nonisotropic Reynolds stress in a non-circular cross sectional flow caused significant change in primary flow field and secondary flow field. The exprimental results were presented as a basic data for the progress of turbulence closure models in complex flow geometries.

1. Introduction

The use of heat transfer surface of non-circular shape in heat exchanger design has increased greatly due to a recent trend toward more compact heat exchanger. Turbulent flows in non-circular ducts have been special interest because they present a particular flow situation, where the secondary flow of Prandtl's second kind appears and distorts considerably the primary flow field. Recently, Launder — Ying[5], Gessner et al.[4] and many other investigators proposed turbulence closure models in non-circular duct flows. Almost all of them focused their attension on a square duct turbulent flow or a turbulent boundary layer along a corner intersecting at right angles. Considerable amounts of experimental results are available at the present stage. These experimental results have been properly compared with the prediction to check the validity of proposed turbulence closure models in complex flow geometries. In addition to the above mentioned experimental results, experiments in other shape of cross section have been expected to compare with the theoretical predictions, because they should certify more wide appricability of the turbulence closure models.

The purpose of this work is to provide a set of turbulence measurement data of fully developed turbulent flow in an isosceles triangular duct with a narrow apex angle. The results obtained in this work may deserve to be a basic data for the progress of turbulence closure models in complex flow geometries. The presentation of experimental results in non-circular cross sectional flow is fairly difficult task. Usually contour plots of some flow characteristics are used. This presentation method is useful for the qualitative understanding of the overall flow pattern. However, quantitative comparison with the theoretical predictions is almost impossible if one wants to read out a numerical data from such a contour plot figure. Thus, in this study, all set of numerical data are presented as the tables. Comparison of these experimental results with theoretical predictions will be discussed in the forthcoming paper by the present

* Department of Chemical Enginneering
** Graduate Student, Chemical Engineering

authors[8]. In addition to the data presentation, the reliability of experimental method will be discussed in this study. For this purpose, the same measuring system was applied to the fully developed turbulent flow in a round tube. The experimental results are compared with the well accepted data of Lawn[6] in the same flow geometry.

2. Experimental Apparatus and Procedure

The schematic diagram of experimental apparatus is shown in Fig. 1. The dimensions of test duct are shown in this diagram. The hydraulic diameter, D_h, of the

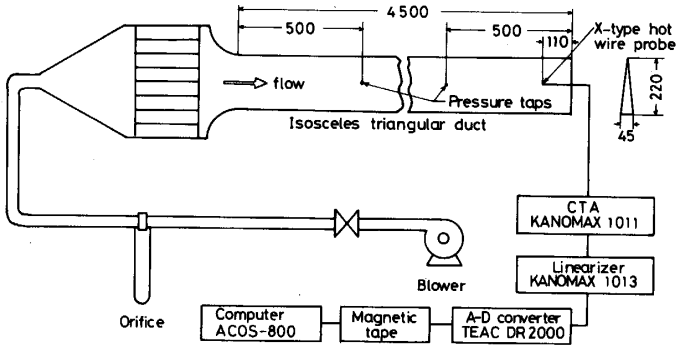

Fig. 1 Experimental apparatus.

isosceles triangular duct was 40.6 mm, and the apex angle, θ, was 11.6 degree. As a preliminary experiment, longitudinal pressure drop, ΔP, was measured using the pressure taps located on the side wall. Another preliminary experiment was the measurement of longitudinal velocity profile over the whole cross section of test duct. This measurement was attempted to check the symmetry of the flow field. A hot wire anemometer and additional data acquisition system shown in Fig. 1 were used to measure the fluctuating velocity components. The measuring positions are indicated in Fig. 2 by small dots. This diagram shows also the coordinate system employed in this study. The reliability of present hot wire anemometry was certified by applying this measuring system to a fully developed turbulent flow in a round tube. For this purpose, a round rube (75 mm inner dia. and 5 m long) was used as a test tube.

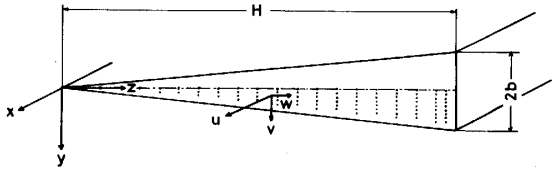

Fig. 2 Coordinate system (small dots indicate the measuring points by a hot wire anemometer).

Test fluid of this experiment was air (density, $\rho = 1.186$ kg/m^3, kinematic viscosity, $\nu = 1.545 \times 10^{-5}$ m^2/s). Single Reynolds number, Re ($= D_h U_0/\nu$), of 10,400 was employed as a experimental condition for hot wire anemometry. At this Reynolds number, the average velocity, U_0, friction factor, f, and average friction velocity, u^*, were 3.96 m/s, 0.00671 and 0.229 m/s, respectively.

3. Results and Discussion

3–1 *Longitudinal pressure distribution*

Longitudinal pressure distribution was measured by a two liquids (toluene — water) micro pressure meter of which minimum reading was 0.04 Pa. The results are shown in Fig. 3. Pressure gradient, $\Delta P/dz$, is almost constant for all Reynolds number if $z/D_h > 70$. Thus it is concluded that fully developed condition is satisfied at the velocity measuring position (at $z/D_h = 108$). Friction factor was calculated from the constant value of dP/dz, and plotted against Re in Fig. 4. The results are in good agreement with the previous data given by Carlson — Irvine[2] and Usui et al.[7] for the same duct geometry. The averaged wall shear velocity, u^*, was calculated from the measured friction factor.

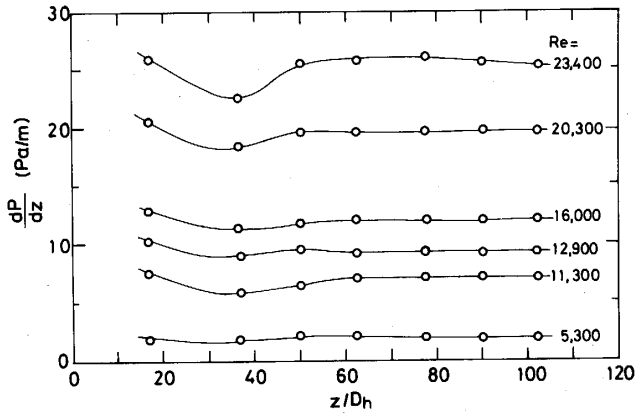

Fig. 3 Distribution of pressure gradient along the longitudinal direction.

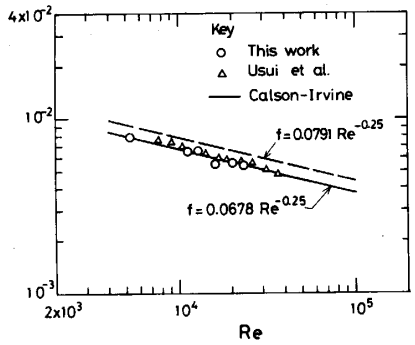

Fig. 4 Dependence of friction factor on Reynolds number.

3–2 *Flow symmetry at the test section*

If alignment of test duct is not accurate, or if side walls of an isosceles triangular duct do not have the same length, the flow field may be affected severely, and experimental results obtained in such an apparatus may have no meaning. Present test duct was constructed on a rigid box beam, and a great deal of care was taken to accomplish the above mentioned conditions. The symmetry of flow field was acertained by measuring the local velocity, $\overline{U}$, using a Pitot tube. Although hot wire anemometry was also employed for velocity measurements, the results were not conclusive because of the change of sensitivity of a hot wire during the experimental time. Thus the local velocity measured by a Pitot tube was used to calibrate the sensitivity of hot wire anemometry. The velocity distribution at several cross sections are shown in Fig. 5. This diagram shows that the flow field at the test section is fairly symmetrical.

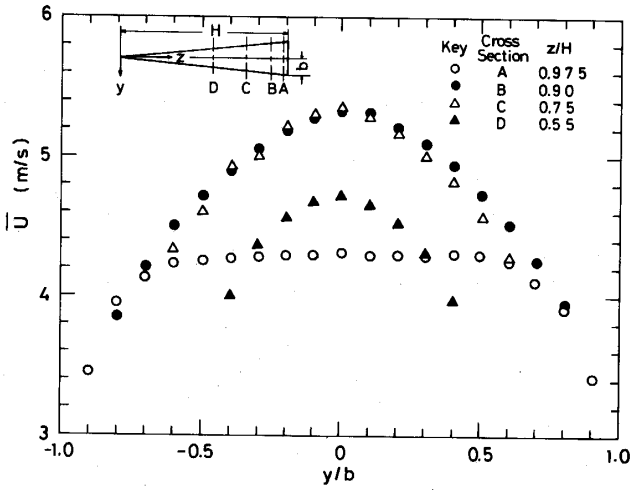

Fig. 5 Check of the symmetry of longitudinal velocity field (results obtained by a Pitot tube at $Re=10{,}200$).

3–3 *Reliability of present hot wire anemometry*

Although recent commercial anemometer has good accuracy, the reliability of combined data acquisition system shown in Fig. 1 should be checked comparing with the well accepted previous data. For this purpose, as stated in the previous section, a fully developed turbulent flow in a round tube was selected. The dimension of test tube have already been described. A X-type hot wire probe (Kanomax model 0252) with 5 μm tangsten wires was used. Sampling frequency and sampling time were 2000 Hz and 6 sec., respectively. This sampling condition was the same all through the present experiments. It may be better to take longer sampling time. However, comparison of the data with various kinds of data size (2000 Hz $\times$ 1 $\sim$ 15 sec) showed that the present sampling condition was enough to obtain correct results of turbulent intensity, Reynolds stresses and dissipation rate of turbulent kinetic energy at $Re=10^4$ in a triangular duct flow. Turbulent intensity, thus obtained in a round tube flow, is shown in Fig. 6. Present results are in good agreement with previously well accepted data of Lawn[6]. The results of axial velocity and Reynolds stress were also in good agreement with Lawn's data, although their comparison is not presented here because of space limitation.

The rate of dissipation of turbulent kinetic energy, ε, was determined following the prodecure given by Lawn[6]. According to the proposal of Bradshaw[1], Lawn recommended following formula to give an estimate of the dissipation rate.

$$E_1(k_1)=0.53\varepsilon^{\frac{2}{3}}k_1^{-\frac{5}{3}} \tag{1}$$

where k_1 is the wave number at inertial subrange and $E_1(k_1)$ is one-dimensional energy spectrum. Actually the value of k_1 is determined in one-dimensional energy spectrum diagram, shown for example in Fig. 7, by fitting tangents of slope $-\frac{5}{3}$ by eye. Although the determination of the contact point with the tangential line seems to be difficult, calculated value of ε is rather insensitive to the location of contact point. For

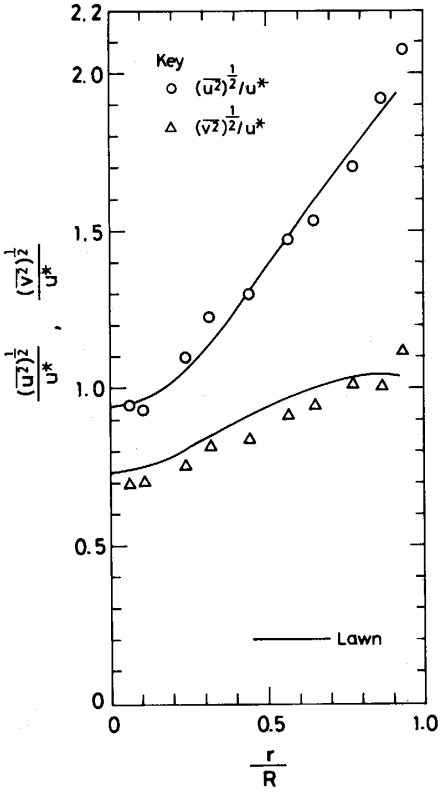

Fig. 6 Turbulent intensity profiles at $Re=$ 24,500 (r is radial distance and R is pipe radius).

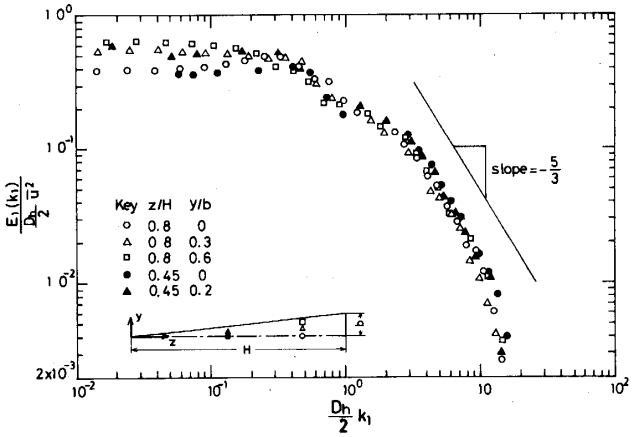

Fig. 7 One-dimensionalenergy spectrum determined from the longitudinal fluctuating velocity.

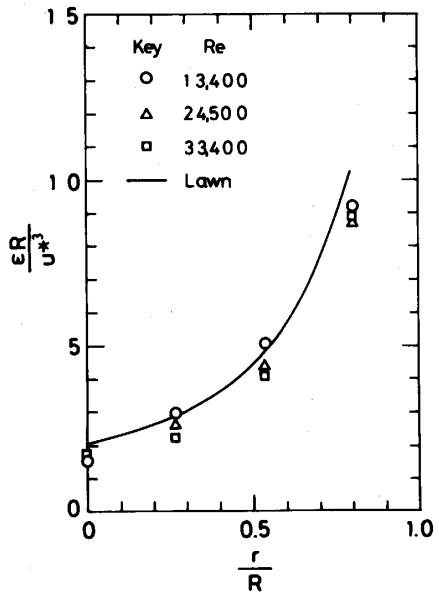

Fig. 8 Distribution of rate of dissipation in a round tube turbulent flow.

example, if one determined the contact point at $D_h k_1/2=4\sim8$, the values of ε scattered about $\pm20\%$ around the mean value. This scatter was also caused by experimental error of one-dimensional energy spectrum. Thus the error estimation can not be correctly done at the present stage. The mean value at several points contained in this fitting zone was employed the rate of dissipation. The experimental results of ε in a round tube flow are compared with Lawn's data in Fig. 8. This diagram indicates that present data analysis for determination of ε is quite reasonable. Once the rate of dissipation is obtained, micro scale of turbulence, λ, is easily calculated by following equation which is based on the assumption of isotropic turbulence,

$$\varepsilon=15\nu\frac{\overline{u^2}}{\lambda^2} \tag{2}$$

The maximum micro scale in a triangular duct flow of this experiment had the value of ca. 3 mm at $Re=10^4$. The wire length of hot wire probe of this experiment was 1.3 mm and was less than the micro scale of turbulence determined from rate of dissipation.

3–4 *Turbulent flow characteristics in isosceles triangular duct*

The experimental results of axial velocity, $\overline{U}$, secondary flow components, $\overline{V}$ and $\overline{W}$ are shown in Table 1, 2 and 3, respectively. A 45° inclined hot wire probe was used for the measurements of secondary flow. This probe was rotated at the measuring

Table 1. Distribution of longitudinal velocity, $\overline{U}$ [m/s].

				y/b					
z/H	0	0.1	0.2	0.3	0.4	0.5	0.6	0.7	0.8
0.975	3.78	3.77	3.79	3.78	3.78	3.69	3.67	3.63	3.60
0.95	4.59	4.60	4.62	4.61	4.60	4.56	4.45	4.23	3.88
0.90	5.37	5.33	5.28	5.14	5.03	4.79	4.57	4.22	
0.85	5.41	5.35	5.32	5.15	4.96	4.79	4.47	4.06	
0.80	5.45	5.37	5.26	5.12	4.93	4.71	4.42		
0.75	5.43	5.37	5.26	5.10	4.87	4.63	4.24		
0.70	5.32	5.27	5.12	4.96	4.76	4.45			
0.65	5.14	5.08	4.93	4.78	4.51	4.24			
0.60	4.97	4.89	4.75	4.52	4.24				
0.55	4.72	4.68	4.48	4.27	3.96				
0.50	4.48	4.41	4.26	3.98					
0.45	4.33	4.24	4.05	3.82					
0.40	3.91	3.83	3.62						
0.35	3.61	3.51	3.27						
0.30	3.31	3.19							
0.25	3.20	3.90							
0.20	2.98								
0.15	2.64								
0.10	1.36								

Table 2. Distribution of secondary flow component, $\bar{V}$ [m/s].

	y/b								
	0	0.1	0.2	0.3	0.4	0.5	0.6	0.7	0.8
0.975	−0.006	−0.015	−0.033	−0.024	−0.036	0.018	0.024	0.042	0.030
0.95	0.003	0.009	0.027	0.040	0.046	0.052	0.052	0.058	0.034
0.90	0.006	0.006	*	0.005	*	−0.003	−0.003	−0.003	
0.85	*	−0.006	−0.006	−0.009	−0.018	−0.018	−0.006	−0.006	
0.80	*	−0.003	−0.003	−0.005	−0.007	−0.005	−0.003		
0.75	*	−0.006	−0.006	−0.003	0.003	−0.003	0.009		
0.70	*	*	*	*	*	−0.009			
0.65	*	*	0.003	0.003	−0.003	0.003			
0.60	−0.006	*	0.005	*	*				
0.55	0.003	0.003	0.006	*	−0.003				
0.50	*	*	−0.003	−0.003					
0.45	*	*	*						
0.40	−0.003	0.003	−0.003						
0.35	*	*	*						
0.30	−0.003	*							
0.25	*	*							
0.20	*								
0.15	*								
0.10	*								

* The data less than 0.1% of averaged velocity U_0 was unreliable, and these data are indicated by "*"

Table 3. Distribution of secondary flow component, $\bar{W}$ [m/s].

	y/b								
z/H	0	0.1	0.2	0.3	0.4	0.5	0.6	0.7	0.8
0.975	−0.018	−0.018	−0.006	0.012	0.012	0.021	0.015	0.018	0.018
0.95	−0.012	−0.015	0.006	0.018	0.031	0.037	0.031	−0.012	−0.061
0.90	0.036	0.042	0.030	0.024	0.012	−0.006	−0.021	−0.068	
0.85	0.024	0.024	0.012	0.006	0.009	−0.012	−0.040	−0.042	
0.80	*	*	*	*	−0.005	−0.007	−0.013		
0.75	−0.012	−0.012	−0.003	*	0.003	*	0.013		
0.70	−0.012	−0.018	−0.008	0.003	0.009	0.006			
0.65	−0.029	−0.020	−0.008	*	0.009	0.009			
0.60	−0.028	−0.027	−0.008	*	0.011				
0.55	−0.033	−0.027	−0.015	*	0.009				
0.50	−0.035	−0.025	−0.006	0.006					
0.45	−0.037	−0.014	−0.003	*					
0.40	−0.040	−0.003	*						
0.35	−0.042	−0.006	*						
0.30	−0.048	−0.013							
0.25	−0.058	*							
0.20	−0.027								
0.15	−0.027								
0.10	*								

* The data less than 0.1% of averaged velocity U_0 was unreliable, and these data are indicated by "*"

Table 4. Distribution of turbulent intensity, $\sqrt{\overline{u^2}}$ [m/s].

					y/b				
z/H	0	0.1	0.2	0.3	0.4	0.5	0.6	0.7	0.8
0.975	0.471	0.441	0.462	0.450	0.457	0.431	0.397	0.398	0.440
0.95	0.391	0.395	0.392	0.377	0.354	0.361	0.364	0.423	0.509
0.90	0.247	0.277	0.304	0.337	0.380	0.409	0.446	0.492	
0.85	0.260	0.281	0.326	0.335	0.405	0.435	0.455	0.544	
0.80	0.245	0.279	0.319	0.347	0.403	0.421	0.496		
0.75	0.242	0.274	0.312	0.358	0.401	0.454	0.516		
0.70	0.250	0.277	0.323	0.381	0.414	0.478			
0.65	0.247	0.288	0.336	0.377	0.424	0.517			
0.60	0.254	0.286	0.320	0.413	0.447				
0.55	0.248	0.283	0.337	0.391	0.500				
0.50	0.240	0.291	0.332	0.414					
0.45	0.243	0.292	0.356	0.430					
0.40	0.240	0.303	0.361						
0.35	0.243	0.300	0.386						
0.30	0.240	0.315							
0.25	0.246	0.371							
0.20	0.268								
0.15	0.279								
0.10	0.173								

Table 5. Distribution of turbulent intensity, $\sqrt{\overline{v^2}}$ [m/s].

					y/b				
z/H	0	0.1	0.2	0.3	0.4	0.5	0.6	0.7	0.8
0.975	0.334	0.312	0.320	0.321	0.305	0.299	0.286	0.259	0.245
0.95	0.273	0.264	0.249	0.254	0.242	0.232	0.231	0.241	0.261
0.90	0.173	0.175	0.190	0.200	0.213	0.231	0.250	0.266	
0.85	0.174	0.180	0.190	0.205	0.225	0.235	0.248	0.281	
0.80	0.169	0.172	0.187	0.193	0.212	0.233	0.252		
0.75	0.166	0.175	0.183	0.199	0.220	0.236	0.256		
0.70	0.166	0.178	0.185	0.204	0.220	0.242			
0.65	0.166	0.170	0.187	0.203	0.228	0.257			
0.60	0.163	0.170	0.190	0.208	0.239				
0.55	0.160	0.168	0.187	0.204	0.243				
0.50	0.159	0.172	0.180	0.211					
0.45	0.157	0.164	0.182	0.207					
0.40	0.152	0.154	0.177						
0.35	0.140	0.149	0.171						
0.30	0.124	0.139							
0.25	0.116	0.131							
0.20	0.099								
0.15	0.064								
0.10	0.018								

Table 6. Distribution of turbulent intensity, $\sqrt{\overline{w^2}}$ [m/s].

					y/b				
z/H	0	0.1	0.2	0.3	0.4	0.5	0.6	0.7	0.8
0.975	0.277	0.270	0.265	0.254	0.257	0.248	0.240	0.255	0.291
0.95	0.234	0.228	0.232	0.227	0.229	0.232	0.248	0.282	0.239
0.90	0.173	0.185	0.203	0.219	0.248	0.276	0.296	0.327	
0.85	0.172	0.188	0.208	0.229	0.263	0.290	0.308	0.346	
0.80	0.164	0.180	0.204	0.234	0.255	0.290	0.328		
0.75	0.167	0.179	0.208	0.234	0.263	0.295	0.351		
0.70	0.171	0.184	0.210	0.232	0.273	0.319			
0.65	0.170	0.190	0.219	0.242	0.280	0.343			
0.60	0.175	0.190	0.221	0.243	0.293				
0.55	0.174	0.188	0.213	0.253	0.314				
0.50	0.172	0.189	0.219	0.269					
0.45	0.172	0.191	0.227	0.264					
0.40	0.168	0.190	0.221						
0.35	0.164	0.185	0.220						
0.30	0.151	0.180							
0.25	0.143	0.189							
0.20	0.130								
0.15	0.121								
0.10	0.042								

Table 7. Distribution of turbulent kinetic energy,

$$k\left(=\frac{1}{2}(\overline{u^2}+\overline{v^2}+\overline{w^2})\right)\ [\mathrm{m^2/s^2}].$$

					y/b				
z/H	0	0.1	0.2	0.3	0.4	0.5	0.6	0.7	0.8
0.975	0.209	0.203	0.210	0.206	0.192	0.175	0.163	0.154	0.165
0.95	0.149	0.144	0.135	0.133	0.194	0.160	0.128	0.153	0.199
0.90	0.059	0.066	0.080	0.098	0.118	0.145	0.168	0.193	
0.85	0.060	0.074	0.085	0.106	0.134	0.152	0.184	0.217	
0.80	0.059	0.068	0.086	0.103	0.129	0.159	0.190		
0.75	0.057	0.069	0.084	0.107	0.130	0.161	0.203		
0.70	0.059	0.070	0.090	0.109	0.139	0.177			
0.65	0.058	0.071	0.093	0.113	0.147	0.195			
0.60	0.059	0.068	0.095	0.119	0.154				
0.55	0.059	0.066	0.092	0.120	0.170				
0.50	0.056	0.080	0.093	0.133					
0.45	0.054	0.069	0.094	0.129					
0.40	0.052	0.066	0.095						
0.35	0.049	0.065	0.100						
0.30	0.043	0.063							
0.25	0.048	0.066							
0.20	0.047								
0.15	0.041								
0.10	0.007								

Table 8. Distribution of Reynolds stress, $\overline{uv}$ [m²/s²].

	y/b								
z/H	0	0.1	0.2	0.3	0.4	0.5	0.6	0.7	0.8
0.975	−0.0065	−0.0077	−0.0113	−0.0118	−0.0079	−0.0073	0.0011	0.0158	0.0278
0.95	−0.0048	−0.0070	−0.0046	0.0	0.0067	0.0184	0.0276	0.0413	0.0521
0.90	0.0004	0.0090	0.0176	0.0256	0.0346	0.0430	0.0502	0.0606	
0.85	−0.0006	0.0120	0.0176	0.0281	0.0396	0.0448	0.0508	0.0639	
0.80	0.0	0.0736	0.0211	0.0260	0.0359	0.0439	0.0521		
0.75	0.0009	0.0105	0.0180	0.0286	0.0379	0.0429	0.0474		
0.70	0.0012	0.0120	0.0189	0.0287	0.0388	0.0439			
0.65	−0.0017	0.0097	0.0211	0.0307	0.0399	0.0460			
0.60	0.0	0.0097	0.0233	0.0321	0.0415				
0.55	0.0	0.0107	0.0203	0.0295	0.0408				
0.50	0.0010	0.0125	0.0203	0.0325					
0.45	0.0	0.0110	0.0204	0.0309					
0.40	0.0020	0.0102	0.0218						
0.35	0.0006	0.0101	0.0186						
0.30	0.0006	0.0093							
0.25	−0.0006	0.0082							
0.20	−0.0015								
0.15	−0.0007								
0.10	−0.0007								

Table 9. Distribution of Reynolds stress, $\overline{uw}$ [m²/s²].

	y/b								
z/H	0	0.1	0.2	0.3	0.4	0.5	0.6	0.7	0.8
0.975	0.0612	0.0534	0.0551	0.0509	0.0526	0.0442	0.0334	0.0342	0.0350
0.95	0.0413	0.0401	0.0389	0.0335	0.0253	0.0202	0.0172	0.0249	0.0443
0.90	0.0068	0.0076	0.0059	0.0026	0.0027	0.0066	0.0026	0.0066	
0.85	0.0029	0.0061	0.0109	0.0100	0.0085	0.0127	0.0157	0.0337	
0.80	0.0017	0.0022	0.0049	0.0063	0.0096	0.0090	0.0176		
0.75	−0.0011	−0.0002	0.0004	0.0033	0.0031	0.0058	0.0330		
0.70	−0.0019	−0.0013	−0.0017	0.0053	0.0022	0.0124			
0.65	−0.0038	−0.0034	−0.0034	0.0011	0.0035	0.0274			
0.60	−0.0064	−0.0041	−0.0025	−0.0047	0.0126				
0.55	−0.0073	−0.0044	−0.0030	0.0013	0.0281				
0.50	−0.0083	−0.0036	−0.0003	0.0082					
0.45	−0.0014	−0.0036	0.0018	0.0101					
0.40	−0.0053	0.0007	0.0017						
0.35	−0.0036	0.0043	0.0086						
0.30	−0.0019	0.0027							
0.25	−0.0011	0.0158							
0.20	0.0049								
0.15	0.0055								
0.10	−0.0005								

Table 10. Rate of Production of turbulent kinetic energy, $-\left(\overline{uv}\frac{\partial \bar{U}}{\partial y}+\overline{uw}\frac{\partial \bar{U}}{\partial z}\right)$ $[m^2/s^3]$.

	y/b								
z/H	0	0.1	0.2	0.3	0.4	0.5	0.6	0.7	0.8
0.95	3.55	3.38	3.05	2.44	1.78	1.69	3.35	6.02	10.8
0.90	0.18	0.36	0.95	1.52	2.80	4.79	6.00	6.91	
0.85	0	0.29	0.90	1.86	3.42	5.03	6.40	9.56	
0.80	0	0.21	1.01	1.93	3.76	4.80	8.40		
0.75	0.07	0.33	0.96	2.25	3.92	5.41	6.67		
0.70	0.02	0.44	1.24	2.51	4.88	6.04			
0.65	0.06	0.45	1.47	3.06	4.71	7.44			
0.60	0.13	0.60	1.92	3.55	5.73				
0.55	0.16	0.75	1.78	3.96	6.54				
0.50	0.20	0.85	2.22	4.68					
0.45	0.19	0.81	2.40	4.71					
0.40	0.15	0.73	2.55						
0.35	0.11	0.75	2.79						
0.30	0.04	0.95							
0.25	0.02	1.51							
0.20	−0.11								
0.15	−0.40								
0.10	0.15								

Table 11. Rate of dissipation of turbulent kinetic energy, ε $[m^2/s^3]$.

	y/b								
z/H	0	0.1	0.2	0.3	0.4	0.5	0.6	0.7	0.8
0.975	7.18	6.87	6.66	7.68	6.46	7.78	7.58	5.03	5.19
0.95	3.33	4.11	3.23	4.92	3.11	3.80	4.30	5.52	9.74
0.90	1.36	1.45	2.00	2.43	3.10	3.80	5.04	6.58	
0.85	1.43	1.60	1.92	2.64	2.89	4.21	6.00	9.22	
0.80	1.04	1.73	2.06	2.53	3.56	4.63	6.96		
0.75	1.15	1.47	1.78	2.71	3.71	5.24	7.57		
0.70	1.25	1.48	2.10	3.07	4.26	5.56			
0.65	1.12	1.74	2.24	3.40	5.00	7.90			
0.60	1.26	1.66	2.30	3.85	5.50				
0.55	1.17	1.63	2.44	4.30	6.90				
0.50	1.21	1.56	2.55	4.78					
0.45	1.08	1.70	2.93	4.84					
0.45	1.08	1.70	2.93	4.84					
0.40	1.12	1.25	2.95						
0.35	0.77	1.70	3.07						
0.30	0.71	1.69							
0.25	0.79	1.39							
0.20	0.34								
0.15	0.02								
0.10	0.01								

position, and the output difference between before and after the rotation of 180° was used to calculate secondary flow velocity component. This experimental technique is reported elsewhere, for example see Ref. 3. Rather long sampling time was needed in this case, typically 2~3 minites of sampling time was taken. A digital voltmeter with long integral time was used to read the difference between two outputs. Turbulent intensities in the three directions, $\sqrt{\overline{u^2}}$, $\sqrt{\overline{v^2}}$ and $\sqrt{\overline{w^2}}$ are shown in Table 4, 5 and 6, respectively. The distribution of turbulent kinetic energy, k, is shown in Table 7. Reynolds stresses, $\overline{uv}$ and $\overline{uw}$ are shown in Table 8 and 9. The Reynolds stress component, $\overline{vw}$ was not measured in this study. Production and dissipation of turbulent kinetic energy are shown in Table 10 and 11. As mentioned before, discussion on the contour plot diagrams of these data will be presented in the forthcoming paper[8].

4. Conclusion

Fully developed turbulent flow characteristics in an isosceles triangular duct with a narrow apex angle were measured by means of a hot wire anemometer. The reliability of measuring technique and flow facility was certified from the discussion presented in this paper. A set of numerical data was presented for the sake of future development of turbulence closure models in noncircular duct flow.

References

1) Bradshaw, P.: NPL Aero Rep. 1220 (1967)
2) Carlson L. W. and Irvine, Jr., T. F.: ASME Paper No. 60-WA-100 (1963)
3) Eppich, H. M.: M. S. thesis, Univ. Washington (1982)
4) Gessner, F. B. and Eppich, H. M.: Proc. 3rd Symp. Turbulent Shear Flow, Davis pp. 2.25–2.32 (1981
5) Launder, B. E. and Ying, W. M.: Proc. Inst. Mech. Engrs., **187**, 455 (1973)
6) Lawn C. J.: J. Fluid Mech., **48**, 477 (1971)
7) Usui, H., Sano, Y. and Fukuma, H.: Int. J. Heat Mass Transfer, **25**, 615 (1982)
8) Usui, H., Okada, S. and Sano, Y.: Proc. 8th Biennial Symp. Turbulence, VI–1 Missouri — Rolla (1983)